# Surface Alignment and Anchoring Transitions in Nematic Lyotropic Chromonic Liquid Crystal

V. G. Nazarenko,[1] O. P. Boiko,[1,2] H.-S. Park,[2] O. M. Brodyn,[1] M. M. Omelchenko,[2] L. Tortora,[2] Yu. A. Nastishin,[2,] and O. D. Lavrentovich[2,*]

[1]*Institute of Physics, prospect Nauky 46, Kiev-39, 03039, Ukraine*

[2]*Liquid Crystal Institute and Chemical Physics Interdisciplinary Program, Kent State University, Kent, Ohio 44242, USA*

*Institute of Physical Optics, 23 Dragomanov str., Lviv, 79005, Ukraine*

(Received 23 February 2010; revised manuscript received 6 May 2010; published 28 June 2010)

The surface alignment of lyotropic chromonic liquid crystals can not only be planar (tangential) but also homeotropic, with self-assembled aggregates perpendicular to the substrate, as demonstrated by mapping optical retardation and by three-dimensional imaging of the director field. With time, the homeotropic nematic undergoes a transition into a tangential state. The anchoring transition is discontinuous and can be described by a double-well anchoring potential with two minima corresponding to tangential and homeotropic orientation.

DOI: 10.1103/PhysRevLett.105.017801 PACS numbers: 61.30.−v, 42.65.−k, 61.30.St, 68.55.am

Spatial bounding of a liquid crystal (LC) lifts the degeneracy of molecular orientation specified by the director $\hat{\mathbf{n}}$ and sets an "easy axis" $\hat{\mathbf{n}}_0$ at the surface. Deviation of $\hat{\mathbf{n}}$ from $\hat{\mathbf{n}}_0$ requires some work, thus establishing a phenomenon of "surface anchoring" that has been explored extensively for thermotropic LCs [1–11]. For lyotropic LCs, such as water solutions of polyelectrolytes, surfactants, dyes, etc., the studies of anchoring are scarce. The view is that the surface alignment of lyotropic LCs is determined by an excluded volume effect, which favors the longest dimension of building units to be parallel to a substrate [12–15]. We study surface phenomena in nematic lyotropic chromonic LCs (LCLCs), a distinct class of self-assembled LCs formed by water solutions of planklike molecules with polyaromatic cores and ionic peripheral groups [16]. A reversible chromonic assembly and mesomorphism are displayed broadly by dyes, drugs, and nucleotides [16]. In water, the LCLC molecules stack face-to-face, forming elongated aggregates. The aggregates are not fixed by covalent bonds, being polydisperse with an average length $l \propto \sqrt{\phi}\ln(E/k_BT)$ that depends on temperature $T$, volume fraction $\phi$, and stacking energy $E \sim (4\text{–}10)k_BT$ [17]. We demonstrate that in LCLCs, $\hat{\mathbf{n}}_0$ can be either parallel to a substrate (planar or tangential alignment, denoted "$P$") or perpendicular (homeotropic, or $H$ alignment), with discontinuous transitions between the two, thus suggesting that both entropy and anisotropic molecular interactions control the surface phenomena.

We study disodium cromoglycate (DSCG) [16], $C_{23}H_{14}O_{11}Na_2$ (Spectrum Inc, purity 98%), dissolved in water at 15 wt % (mixture $A$) and 12.5 wt % doped with 1.5 wt % of $Na_2SO_4$ (mixture $B$). The $H$ alignment was achieved by treating glass plates with 1% water solution of $N$, $N$-dimethyl-$N$-octadecyl-3-aminopropyl trimethoxysilyl chloride (DMOAP) [2]. The two plates are separated by Mylar strips; the cell thickness $d$ was measured by light interference technique. The cells were filled at $T_{NI}$ + 10 K, sealed with a UV-cured Norland epoxy glue, and cooled down to $T = 298$ K with a rate 5 K/min in a thermal stage HS-1 (Instec, Inc.). We used a LC PolScope for in-plane mapping of optical retardation $R(x, y) = \int_0^d |n_o - n_{\text{eff}}|dz$, where $n_{\text{eff}} = (n_o^{-2}\cos^2\theta + n_e^{-2}\sin^2\theta)^{-1/2}$, $\theta$ is the angle between $\hat{\mathbf{n}}$ and the normal $\hat{\mathbf{z}}$ to the cell, $n_o$ and $n_e$ are the ordinary and extraordinary refractive indices, respectively. At 546 nm and $T = 298$ K, we determined $n_o = 1.37 \pm 0.01$ and $\Delta n_A = n_o - n_e = 0.019 \pm 0.002$ for $A$ and $\Delta n_B = 0.015 \pm 0.002$ for $B$ [18]. To image $\hat{\mathbf{n}}$ $(x, y, z)$, we used fluorescence confocal polarizing microscopy (FCPM), by doping the LCLC with 0.003 wt % of fluorescent acridine orange (AO, Sigma-Aldrich) and probing it with a focused laser beam [19]. The fluorescence intensity depends on the angle between $\hat{\mathbf{n}}$ and polarization $\mathbf{P}$ of light, being maximum for $\mathbf{P} \perp \hat{\mathbf{n}}$ and minimum for $\mathbf{P} \parallel \hat{\mathbf{n}}$, suggesting that AO intercalates between the DSCG molecules.

The initial unaligned texture coarsens and then shows dark expanding nuclei of the $H$ state that fill the entire cell, Fig. 1. The $H$ alignment is stable as verified by applying a strong magnetic field, up to 7 kG, to tilt $\hat{\mathbf{n}}$. Once the field is switched off, the $H$ orientation is restored. After a certain time $\tau_H \approx 10$–20 hours, the LCLC undergoes an $H$-$P$ transition through nucleation and expansion of birefringent domains, Fig. 1(c) and 1(d). These appear not only at the

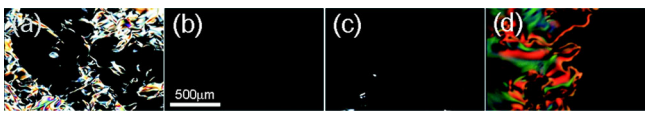


FIG. 1 (color online). Textural evolution viewed between crossed polarizers; mixture $A$, $d = 50$ $\mu$m, $T = 298$ $K$. Dark nuclei of the $H$ state appear at $\tau \approx 10$ min after the isotropic-nematic transition (a), $H$ orientation at $\tau = 25$ min (b); appearance, $\tau = 670$ min (c) and expansion, $\tau = 810$ min (d) of bright $P$ regions.

 

periphery but also in the middle of samples, Fig. 1(c). Two similar cells, one left under normal conditions and another one immersed in a mineral oil, demonstrated similar evolution. Therefore, a possible slow drying is not a major contributor to the effect, although the dynamics of aggregate assembly most certainly is. The *H*-*P* transition might be direct, with $R$ abruptly changing from 0 to $R_{\max} = \Delta n_A d$, line 1, or indirect, with an intermediate step $R \approx \Delta n_A d/2$, lines 2, 3 in Fig. 2(a). The tilt $\beta = \partial R/\partial x$ at the states' boundaries varies broadly, from $\sim$100 nm/$\mu$m, to $\sim$1 nm/$\mu$m. FCPM of the vertical cross sections shows that the boundaries represent sharp walls that are either vertical (large $\beta$) or tilted (small $\beta$). For example, Fig. 2(b) shows a tilted ($\sim$30°) boundary separating an $H$ layer with $\hat{\mathbf{n}}||\hat{\mathbf{z}}$ and a $P$ layer with $\hat{\mathbf{n}}\perp\hat{\mathbf{z}}$; at either of the two $H$ plates, the transition from $\hat{\mathbf{n}}||\hat{\mathbf{z}}$ to $\hat{\mathbf{n}}\perp\hat{\mathbf{z}}$ is abrupt.

To quantify the surface properties further, we use hybrid aligned wedge cells [5], assembled from two *different* plates, an $H$ plate with DMOAP and a $P$ plate with buffed polyimide SE-7511 (Nissan). The dihedral angle is small, <0.1°. The cells show a critical thickness $d_c$ at which $R$ changes abruptly, Fig. 3; $d_c$ varies in the range 5–10 $\mu$m from sample to sample. At $d < d_c$, $\hat{\mathbf{n}}$ is uniform, either in the $H$ state, if the experiment is performed at the beginning of $\tau_H$ for the mixture $A$, or in the $P$ state for the mixture $B$. At $d > d_c$, $\hat{\mathbf{n}}$ is distorted, as evidenced by the tilt $\alpha = \partial R/\partial d$ that is neither 0 nor $\Delta n$, Fig. 3. The behavior of $R$ ($d > d_c$) is complex and depends on the tilt of walls separating the states $\hat{\mathbf{n}} = \text{const}$ and $\hat{\mathbf{n}} \neq \text{const}$. The walls can be vertical, Fig. 4(a), tilted [as in Fig. 2(b)], or practically horizontal, Fig. 4(c). We compare the cross sections of thin and thick parts of the same wedge, Figs. 4(b)–4(d). The thin part is in a uniform $H$ state, with fluorescence equally strong for any in-plane orientation of **P**, Fig. 4(b). In the thick part, Fig. 4(c), the top 1/3 is occupied with an $H$ layer, as evidenced in Fig. 4(d) by an overlap of the fluorescence profiles. In the bottom 2/3, $\hat{\mathbf{n}}$ is close to planar, as the fluorescence is weak, Figs. 4(c) and 4(d).

The experiments suggest that in the studied LCLC, $\hat{\mathbf{n}}_0$ can be either tangential (planar) or homeotropic. The $H$ alignment is stable only within a finite period of time $\tau_H$. The anchoring transitions are strongly discontinuous. The findings are unusual, as lyotropic LCs are notoriously hard to align and when they do align, there are no anchoring transitions. The *H*-*P* transitions occur in thermotropic LCs, but they are continuous there [4,10]. Discontinuous transitions were reported for *in-plane* realignment at anisotropic crystalline substrates [1,8] and for patterned plates with a spatially varying easy axis [11]. As shown by Sluckin and Poniewierski [7], the simplest potential leading to the first-order *H*-*P* transitions in semi-infinite samples is $f_s = W_2(\hat{\mathbf{n}}\cdot\hat{\mathbf{z}})^2 + W_4(\hat{\mathbf{n}}\cdot\hat{\mathbf{z}})^4$. This form also describes well the reorientation of thermotropic LCs by external fields [3,6]. For the $H$ plate with $\hat{\mathbf{n}}_0||\hat{\mathbf{z}}$, $f_s$ can be cast as $W_{2H}\sin^2\theta_H + W_{4H}\sin^4\theta_H$ with the anchoring coefficients $W_{2H} > 0$ and $W_{4H} > -W_{2H}$. The change from $W_{4H} > -W_{2H}$ to $W_{4H} < -W_{2H}$ corresponds to the first-order *H*-*P* transition that has not been observed so far experimentally [9]. Sluckin and Poniewierski [7] expressed $W_{2H}$ and $W_{4H}$ through the temperature-dependent scalar order parameter $S(T)$ so that the transitions were temperature-driven. In our case, the changes in $W_{2H}$ and $W_{4H}$ can be related also to the dynamics of self-assembly. Since the $H$ state is observed after the samples are cooled down from the isotropic phase, it should be accompanied by the growth of aggregates, as $l \propto \sqrt{\phi}\ln(E/k_BT)$. Short and long aggregates might align differently at the substrates, say, normally and tangentially, the entropy effect being one of the reasons.

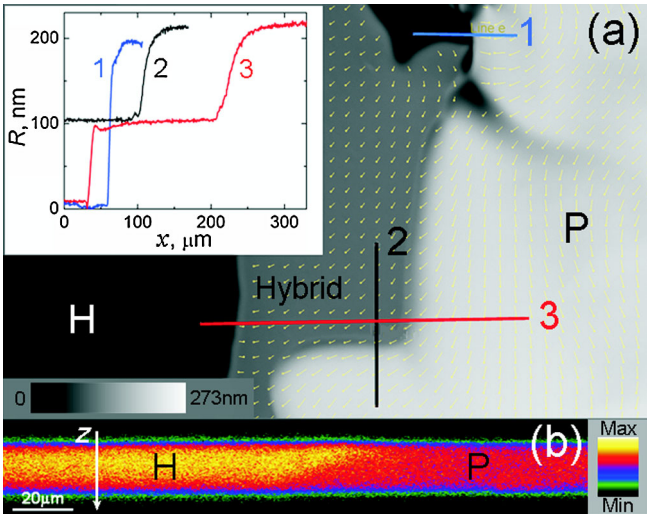


FIG. 2 (color online). *H*-*P* transition in the mixture $A$ viewed as (a) a grey scale map of $R$ in ($x$, $y$) plane of the cell ($d \approx 11$ $\mu$m) and as a variation of $R$ along the lines 1, 2, and 3 (inset); (b) a FCPM vertical cross section of a cell with a tilted boundary.

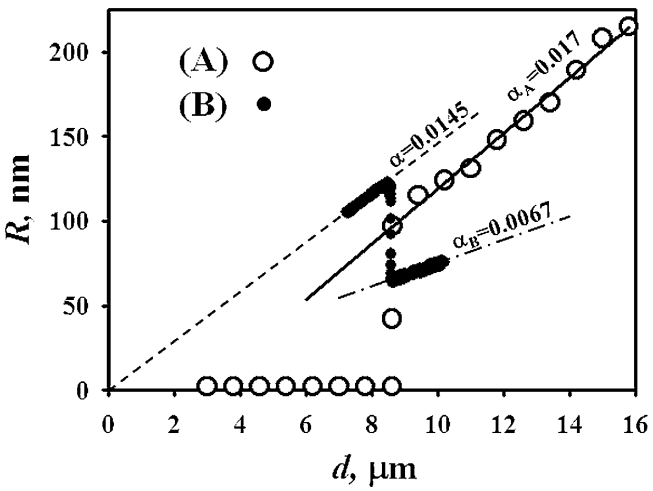


FIG. 3. $R(d)$ for mixtures $A$ and $B$ in the hybrid aligned wedge cells.

For cells of a finite $d$, such as the hybrid aligned wedges, the free energy per unit area should include both anchoring and elastic terms:

$$f = \frac{1}{2}\int_0^d K(\theta)\left(\frac{d\theta}{dz}\right)^2 dz + W_{2H}\sin^2\theta_H + W_{4H}\sin^4\theta_H + W_{2P}\cos^2\theta_P + W_{4P}\cos^4\theta_P, \quad (1)$$

where $K(\theta) = K_1\sin^2\theta + K_3\cos^2\theta$, $K_1$ and $K_3$ are the splay and bend elastic constants; $W_{2P} > 0$ and $W_{4P} > -W_{2P}$, to guarantee $\hat{\mathbf{n}}_0 \perp \hat{\mathbf{z}}$ at the $P$ plate. For $d \to \infty$, the conflicting boundary conditions are satisfied by reorienting $\hat{\mathbf{n}}$ by $\pi/2$. As $d$ decreases, the elastic torque $\propto (\theta_P - \theta_H)/d$, determined by the actual polar angles $\theta_P$ and $\theta_H$ at the plates, becomes stronger, forcing $\theta_P$ and $\theta_H$ to deviate from their "easy" values $\pi/2$ and 0. At some $d_c$, the plate with weaker anchoring might give up, allowing $\hat{\mathbf{n}}$ to be uniform. For analytical treatment, we assume $K_1 = K_3 = K$ and fix $\theta$ at the stronger anchored plate, as supported by FCPM, Figs. 2(b), 4.

For the case $A$ in Fig. 3, $\theta_H = 0$, thus $f = f_P(\theta_P) = K\theta_P^2/(2d) + W_{2P}\cos^2\theta_P + W_{4P}\cos^4\theta_P$. The values of $\theta_P$ that minimize $f_P$ are found from the conditions $\partial f_P/\partial\theta_P = 0$ and $\partial^2 f_P/\partial\theta_P^2 > 0$. When $d \to \infty$ and $W_{4P} < -W_{2P}/2$, $f_P$ has an absolute minimum at $\theta_P = \pi/2$ and a local one at $\theta_P = 0$. The two are separated by a barrier at $\theta_{Pb} = \arccos\sqrt{-\frac{W_{2P}}{2W_{4P}}}$. For a finite $d \gg K/W_{2P}$, $f_P$ with $-1 < W_{4P}/W_{2P} < -1/2$ preserves its double-well features. In particular, $\theta_P = 0$ is still a local minimum. The coordinate $\theta_{P,\min}$ of the absolute minimum, however, becomes smaller than $\pi/2$, because of the elastic torque $\propto \theta_P/d$. We evaluate $f_P$ near $\theta_P \approx \pi/2$ to find $\theta_{P,\min} \approx \frac{\pi}{2}(1 - \frac{K}{2dW_{2P}+K})$. The difference $\Delta f_P = f_P(\theta_{P\min}) - f_P(0)$ vanishes at $d_{cP} \approx \frac{\pi^2 K}{8(W_{2P}+W_{4P})}$. For $d < d_{cP}$, the uniform $H$ state is stable, while for $d > d_{cP}$, the hybrid state has the lowest energy. The transition is discontinuous, with a big jump $\Delta\theta_P \approx \frac{\pi^3}{8(1+W_{4P}/W_{2P})+2\pi^2}$ in the range $1.31 \le \Delta\theta_P \le 1.57$ that corresponds to the limits $-1 < W_{4P}/W_{2P} < -1/2$. Similarly for the case $B$, $\theta_P = \pi/2$ and $f_H(\theta_H) = K(\pi/2 - \theta_H)^2/(2d) + W_{2H}\sin^2\theta_H + W_{4H}\sin^4\theta_H$. At $d$ smaller than $d_{cH} \approx \frac{\pi^2 K}{8(W_{2H}+W_{4H})}$, the uniform $P$ state $\theta(z) = \pi/2$ is stable, and at $d > d_{cH}$, the hybrid state with $\theta_{H\min} = \frac{\pi}{2}\frac{K}{2dW_{2H}+K} \ll 1$ is stable. The transition is discontinuous, with the jump $\Delta\theta_H \approx \frac{\pi^3}{8(1+W_{4H}/W_{2H})+2\pi^2}$ in the range (1.31–1.57). The qualitative features of this analytical description remain intact when the full form of $f$ in Eq. (1) is analyzed numerically.

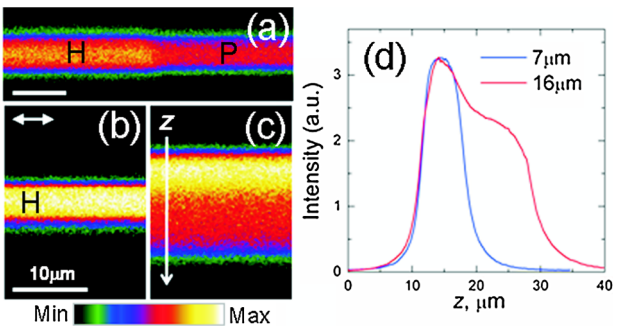


FIG. 4 (color online). Vertical FCPM views of hybrid aligned wedges with mixture $A$; (a) vertical boundary between $H$ and $P$ states, $d = 10$ $\mu$m; (b) homeotropic thin, $d = 7$ $\mu$m and (c) hybrid thick, $d = 16$ $\mu$m, parts of the same wedge and comparison of their fluorescent profiles (d). The double arrow in (b) shows light polarization $\mathbf{P}$.

The model above explains why the thin parts of wedge cells are uniform and why the director orientation at the surfaces is close to 0 and $\pi/2$. The thickness $d_c \sim K/(W_2 + W_4)$ has the meaning of surface extrapolation length, also called the de Gennes–Kleman length. The value $d_c \sim 10$ $\mu$m is of the same order as the one extracted from the experiments on elastic distortions around colloidal inclusions in LCLCs [20]. With $K \sim 10$ pN [21], one estimates $W_2 + W_4 \sim 10^{-6}$ J/m$^2$, which is comparable to the anchoring coefficients found in thermotropic LCs in the regime of "weak" anchoring [2]. The small $W_2 + W_4$ facilitates metastable surface orientations, analogs of the strongly supercooled states. Their transformations into the stable states are hindered by the barriers featured by $f_P$ and $f_H$, and by the surface defects of line tension $\sim K$ that separate the areas with a different director tilt. These defects are seen as cusps in $R(x)$, Fig. 2(a). The nuclei of new alignment should be of a size $\sim K/|\Delta f|$ or larger, to overcome the nucleation barrier $\sim K^2/|\Delta f|$. The maximum $\Delta f$ is $W_2 + W_4$. With $W_2 + W_4 \sim 10^{-6}$ J/m$^2$, the nucleation barrier is large, $\sim K^2/(W_2 + W_4) \sim 10^{-16}$ $J \gg k_B T$, which signals that the metastable states can be long-lived and that nucleation is heterogeneous, assisted by inhomogeneities, Fig. 1.

The general expression $R = \int_0^d |n_o - n_{\text{eff}}|dz$ matches the data in Fig. 3 at $d < d_c$, with $\alpha = 0$ in the $H$ state and $\alpha \approx \Delta n_B = 0.015$ in the $P$ case. For the deformed states at $d > d_c$, the standard model is that $R(d)$ is determined by smooth variations of $\hat{\mathbf{n}}$ with $S = \text{const}$ [5]. Then for the $A$ case, $R_A(\theta_P) = dJ(\theta_P, 0)/I(\theta_P, 0)$, while for the $B$ case, $R_B(\theta_H) = dJ(\pi/2, \theta_H)/I(\pi/2, \theta_H)$, where $J(\zeta, \eta) = \int_\zeta^\eta \sqrt{K(\theta)}(n_o - n_{\text{eff}})d\theta$, $I(\zeta, \eta) = \int_\zeta^\eta \sqrt{K(\theta)}d\theta$ [5]. For $K_1 = K_3 = K$, using the smallness of $\Delta n/n_0$, one finds $R_A(d) = d\Delta n_A(\theta_P - \sin 2\theta_P)/2\theta_P$ and $R_B(d) = d\Delta n_B(\pi - 2\theta_H + \sin 2\theta_H)/(2\pi - 4\theta_H)$. Using the discontinuities of $R$ in Fig. 3, (97 ± 3) nm for $A$ and (64 ± 2) nm for $B$, we conclude that the jumps in $\theta_P$ and $\theta_H$ at $d_c$ are substantial, $\approx$ (1.3–1.57), as expected from the model above. The tilts $\alpha$ are much harder to describe as these are affected by the tilt of boundaries between different states. Assuming a vertical boundary for the cell $B$ and the expression for $R_B(d)$ above, one finds that at $d > d_c$, $\alpha_B = \partial R_B/\partial d = \frac{\Delta n_B}{2}(1 + \frac{\pi^2}{24}\frac{K^3}{W_{2H}^3 d^3}) = 0.0075$ or larger. The experimental $\alpha_B = 0.0067$ is smaller by 10%, Fig. 3. The

difference can be accounted for by the fact that $K_1 < K_3$. Numerical evaluation of $R$ with $K_1 \neq K_3$ shows that $\alpha_B = 0.0067$ corresponds to $K_1/K_3 \approx 0.4$, a reasonable result [21]. The discrepancy between the theoretical $\alpha_A \approx \frac{\Delta n_A}{2}(1 - \frac{K^2}{2W_{2P}^2 d^2}) \lesssim 0.01$ and the experimental $\alpha_A \approx 0.017$ is more significant. It cannot be explained by $K_1/K_3 \neq 1$. To show this, we assumed $\theta_P = \pi/2$ (to maximize the theoretical $\alpha_A$) and then evaluated $R$ for $K_1/K_3 \neq 1$. By changing the ratio $K_1/K_3$ in the range $10^{-5}$ to $10^5$, we find $\alpha_A$ changing from 0.007 to 0.013, still smaller than the experimental value. In principle, $\alpha_A \approx 0.017$ can be obtained by allowing a nonzero $\theta_H \approx 0.1$. However, with $\theta_H \approx 0.1$, the cell retardation should be much higher than in the experiment, e.g., one should measure $R \approx 140$ nm at $d = 8.7$ $\mu$m, and the actual result is only $R \approx 100$ nm, Fig. 3. We thus conclude that $R(d)$ at $d > d_c$ is affected by the tilted sharp boundaries such as the ones in Fig. 2(b) and Figs. 4(c) and 4(d). The boundaries with sharply varying $\hat{\mathbf{n}}$ imply a changing $S$. The latter is expected to happen through the ''interchanging eigenvalues'' of the tensor order parameter in thin hybrid aligned cells [22] with $d \approx \xi_{bx}$, where $\xi_{bx}$ is the biaxial correlation length. In thermotropic nematics, $\xi_{bx} = (10–100)$ nm [22], but in LCLCs, $\xi_{bx}$ can be larger, since the gradients of $S$ can be accommodated by redistribution of short and long aggregates in the intrinsically polydisperse LCLC. The standard approach to calculate $R$ and $\alpha$ is not applicable to the case with a changing $S$.

To conclude, we demonstrated that in the LCLC, surface alignment can be both planar and homeotropic with a strongly discontinuous transition between the two that can be described by a double-well anchoring potential. Much more work is needed to gain an understanding of LCLC behavior at the surfaces and in the bulk, as the study suggests that the LCLC structure is affected by kinetics of self-assembly and that the director distortions can be accompanied by gradients of the scalar order parameter.

We are grateful to the anonymous referees for useful suggestions. The work was supported by NSF Materials World Network on Lyotropic Chromonic Liquid Crystals DMR076290, ARRA DMR 0906751, Ohio Research Cluster on Surfaces in Advanced Materials, NAS of Ukraine Grant No. #1.4.1B/109, Fundamental Research State Fund Project No. UU24/018, and by the Ministry of Education and Science of Ukraine, Project No. 0109U001062.

*olavrent@kent.edu

[1] R. G. Horn, J. N. Israelachvili, and E. Perez, J. Phys. (Orsay, Fr.) **42**, 39 (1981).
[2] J. Cognard, Mol. Cryst. Liq. Cryst. **78**, 1 (1982).
[3] K. H. Yang and C. Rosenblatt, Appl. Phys. Lett. **43**, 62 (1983).
[4] G. E. Volovik and O. D. Lavrentovich, Zh. Eksp. Teor. Fiz. **85**, 1997 (1983); [Sov. Phys. JETP **58**, 1159 (1983)].
[5] G. Barbero, N. V. Madhusudana, J. F. Palierne, and G. Durand, Phys. Lett. A **103**, 385 (1984).
[6] H. Yokoyama and H. A. van Sprang, J. Appl. Phys. **57**, 4520 (1985).
[7] T. J. Sluckin, A. Poniewierski, in *Fluid Interfacial Phenomena*, edited by. C. A. Croxton (John Wiley and Sons, Chichester, 1986).
[8] J. Bechhoefer, J.-L. Duvail, L. Masson, B. Jérôme, R. M. Hornreich, and P. Pieranski, Phys. Rev. Lett. **64**, 1911 (1990).
[9] S. Faetti, in *Physics of Liquid Crystalline Materials*, edited by. I.-C. Khoo and F. Simoni (Gordon and Breach, New York, 1991).
[10] J. S. Patel and H. Yokoyama, Nature (London) **362**, 525 (1993).
[11] B. Zhang, F. K. Lee, O. K. C. Tsui, and P. Sheng, Phys. Rev. Lett. **91**, 215501 (2003).
[12] R. B. Meyer, in *Polymer Liquid Crystals*, edited by A. Ciferri, W. R. Krigbaum, and R. B. Meyer (Academic Press, New York, 1982).
[13] A. Poniewierski and R. Hołyst, Phys. Rev. A **38**, 3721 (1988).
[14] M. F. Sharlow and W. M. Gelbart, Liq. Cryst. **11**, 25 (1992).
[15] P. Poulin, N. Frances, and O. Mondain-Monval, Phys. Rev. E **59**, 4384 (1999).
[16] J. Lydon, Curr. Opin. Colloid Interface Sci. **8**, 480 (2004).
[17] A. J. Dickinson, N. D. LaRacuente, C. B. McKitterick, and P. J. Collings, Mol. Cryst. Liq. Cryst. **509**, 9 (2009).
[18] Yu. A. Nastishin, H. Liu, T. Schneider, V. Nazarenko, R. Vasyuta, S. V. Shiyanovskii, and O. D. Lavrentovich, Phys. Rev. E **72**, 041711 (2005).
[19] O. D. Lavrentovich, Pramana J. Phys. **61**, 373 (2003).
[20] S. V. Shiyanovskii, T. Schneider, I. I. Smalyukh, T. Ishikawa, G. D. Niehaus, K. J. Doane, C. J. Woolverton, and O. D. Lavrentovich, Phys. Rev. E **71**, 020702(R) (2005).
[21] Yu. A. Nastishin, K. Neupane, A. R. Baldwin, O. D. Lavrentovich, and S. Sprunt, Electronic Liquid Crystal Communications, July 15 (2008).
[22] P. Palffy-Muhoray, E. C. Gartland, and J. R. Kelly, Liq. Cryst. **16**, 713 (1994); H. G. Galabova, N. Kothekar, and D. W. Allender, Liq. Cryst. **23**, 803 (1997); A. Šarlah and S. Žumer, Phys. Rev. E **60**, 1821 (1999); C. Chiccoli, P. Pasini, A. Šarlah, C. Zannoni, and S. Žumer, Phys. Rev. E **67**, 050703(R) (2003); P. I. C. Teixeira, F. Barmes, C. Anquetil-Deck, and D. J. Cleaver, Phys. Rev. E **79**, 011709 (2009); D. de las Heras, L. Mederos, and E. Velasco, Phys. Rev. E **79**, 011712 (2009).